Journal of Alloys and Compounds 509 (2011) 7927–7930

Contents lists available at ScienceDirect

Journal of Alloys and Compounds

journal homepage: www.elsevier.com/locate/jallcom

Formation and properties of SrB_6 single crystals synthesized under high pressure and temperature

Shengwei Xin, Shaocun Liu, Nan Wang, Xianyue Han, Limin Wang, Bo Xu, Yongjun Tian, Zhongyuan Liu, Julong He, Dongli Yu*

State Key Laboratory of Metastable Materials Science and Technology, Yanshan University, Qinhuangdao, Hebei 066004, People's Republic of China

ARTICLE INFO

Article history:
Received 10 December 2010
Received in revised form 6 May 2011
Accepted 10 May 2011
Available online 19 May 2011

Keywords:
High pressure
SrB6
Semi-metallic
Single crystals

ABSTRACT

Pure SrB_6 single crystals are synthesized under high pressure (5 GPa) and temperature (1300 °C). The structure and morphology of the SrB_6 single crystals are characterized by X-ray diffraction and field emission scanning electron microscope. The lattice constant of the SrB_6 crystals with a space group of *Pm*-3*m* is $a = 4.1975$ Å. The dependence of electric resistivity and Hall coefficient on temperatures from 2 to 300 K show that the SrB_6 single crystals are conductive materials with semi-metallic behavior and can be considered as electronic current carriers. The results of the band structure calculation show that the conduction and valence bands meet at the *X* point at the Fermi Level, which is consistent with the experimentally measured conducting behavior of SrB_6 single crystals. The total and partial density of states show that the states at the Fermi level come from the 2p orbitals of the B atoms and the 4d orbital of the Sr atom. The magnetization measurement shows the diamagnetic nature of the SrB_6. The nanoindentation measurement indicates that the hardness of SrB_6 reached 33 GPa.

1. Introduction

Strontium hexaboride is well-known for its excellent properties, such as high melting temperature (2235 °C), high hardness, and low coefficient of thermal conductivity [1,2]. It is also extensively utilized for high temperature insulation, nuclear reactor control rods [1,2].

Although no magnetic elements are present in the CaB_6 crystals, weak ferromagnetism have been observed at high temperatures ($T_c = 600$ K). Nearly identical magnetic effects with $Sr_{1-x}La_xB_6$, and $Ba_{1-x}La_xB_6$ have also been found, along with the maximum moment identified at $x = 0.005$ [3]. In the beginning, this weak ferromagnetism was considered to be the spontaneous ferromagnetism of low-density electron gas which is due to the conduction electrons introduced by La doping [4]. Later, the ferromagnetism was discovered in the undoped SrB_6 [5,6], raising new questions about the origin of the unusual magnetism.

Meanwhile, the electronically conductive nature of SrB_6 still remains unknown. Both semiconducting [7,8] and semimetallic [9–11] behaviors have been observed in experiments and theoretical calculations on SrB_6. A study using both angle-resolved photoemission spectroscopy and *k*-resolved resonant inelastic X-ray scattering have revealed an *X*-point band gap of >1 eV for SrB_6 [7]. Based on the results of electrical resistivity investigations at both zero and non-zero frequencies above ^{4}He temperatures, SrB_6 is close to being a semiconductor [8]. However, it also possesses metallic behavior below 0.5 K. On the other hand, both the local density approximation [9] and generalized gradient approximation [10] band structure calculations have predicted the occurrence of overlapping bands, indicating that SrB_6 is semimetallic. In addition, the result of de Haas–van Alphen (dHvA) experiment on SrB_6 [11] has been interpreted using the semimetal framework.

Recently, SrB_6 single crystals have been grown through a molten aluminum metal flux method [12,13]. Using this method, SrB_6 single crystals with a variety of shapes and sizes can be obtained. However, traces of aluminum have been found in the examination of the surface of SrB_6 plates [13], implying that the SrB_6 single crystals may be contaminated. Jash et al. have synthesized crystalline SrB_6 nanowires using a low-pressure chemical vapor deposition apparatus [14]. The nanowires consisted of a crystalline SrB_6 core with diameters of 10–50 nm and lengths of 1–10 μm that are surrounded by a thin 1–2 nm amorphous oxide shell.

Currently, few studies exist on the use of pure elements to synthesize SrB_6 single crystals. In the process of synthesizing SrB_6 single crystals using pure Sr and B, an unavoidable difficulty is the violent evaporation of Sr. The high-pressure technique can solve the problem of Sr evaporation. In this study, we prepare cleaner SrB_6 single crystals through the direct reaction of metal Sr with B powders under high pressure and high temperature (HP–HT). The resistivity, Hall coefficient, magnetism, and hardness of the SrB_6

* Corresponding author. Fax: +86 335 8074 545.
E-mail address: ydl@ysu.edu.cn (D. Yu).

0925-8388/$ – see front matter © 2011 Elsevier B.V. All rights reserved.
doi:10.1016/j.jallcom.2011.05.037

single crystals are measured. We also investigated the mechanism of the SrB_6 single crystal conductive behavior using first principles calculations.

2. Samples and experimental methods

Starting with Sr pellets with 99% purity and boron powder with 99.99% purity, pure SrB_6 single crystals were synthesized in a large-volume cubic-anvil press under high pressure (5 GPa) and high temperature (1300 °C) for 3 h. The SrB_6 crystals were formed through the liquid (Sr)–solid (B) state reaction [15] and can be expressed as follows: Sr (l) + B (s) = SrB_6 (s).

The phase identification of the product was carried out using a D8 X-ray powder diffractometer (D8 DISCOVER, Bruker AXS) with Cu Kα radiation and a micro-probe to obtain X-ray information. The morphology of the SrB_6 crystals was characterized by HITACHI S-4800 Field Emission Scanning Electron Microscope (FESEM). Using the Physical Property Measurement System, the electrical resistivity and the Hall-coefficient of the SrB_6 single crystal were measured at a range of 2–300 K using the conventional four-probe method and the five-point-contact technique, respectively. Nanoindentation experiments were performed using the nano mechanical test instruments (TriboIndenter) with a Berkovich diamond tip. The hardness and reduced modulus were determined from indentation curves measured at the different loads of 2000–10,000 μN, in accordance with the method of Oliver and Pharr [16]. The hardness and reduced modulus were calculated from 9 independent measurements. The indentation size and crack length were measured by in situ atomic force microscopy (AFM). The calculations of band structure and density of states (DOS) were performed using density functional theory implemented in CASTEP code. The calculation was based on a Perdew–Burke–Ernzerhof form of the generalized gradient approximation and ultra-soft Vanderbilt potential. The plane-wave cut-off Ecut was 270 eV, and the *k*-point mesh parameters were set to 6 × 6 × 6.

3. Results and discussion

Fig. 1 shows X-ray diffraction patterns along the reflection of the (1 0 0) face of the SrB_6 single crystal (inset). The strongest diffraction peak at 43.07° corresponds to the reflection of the (2 0 0) crystal face. The other two peaks are the reflections of (1 0 0) and (3 0 0) crystal faces, respectively. The lattice constant obtained from the diffraction data is a = 4.1975 Å, which is consistent with a previously reported result (lattice constant: a = 4.1981 Å, space group: Pm-3m) [8].

Fig. 2 shows a typical FESEM image of the synthesized SrB_6 single crystals. The obtained crystals are perfect, and most of them show a rod-like shape with the longest being about 810 μm. The composition of the single crystal determined by the EDS analysis is B and Sr with a ratio of B/Sr = 6.02(±0.08).

The resistivities $\rho(T)$ of SrB_6 at the temperature range of 2–300 K are shown in Fig. 3. The measurement was accomplished using an SrB_6 single crystal measuring 0.15 mm along one axis (Fig. 3, inset (a)). The $\rho(T)$ drops monotonically with the decreasing temperature. The resistivities at 2 K and room temperature are ρ(2 K) = 2.68 mΩ cm and ρ(300 K) = 3.80 mΩ cm, respectively. The residual resistance ratio (RRR) is 1.42. Compared with the metallic

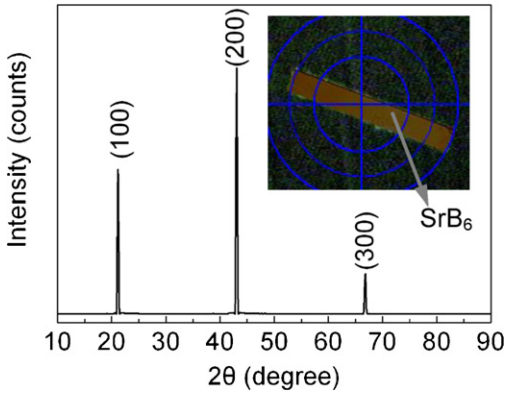

Fig. 1. The XRD pattern of a single SrB_6 crystal. The inset shows a single crystal placed on the Si sample stage.

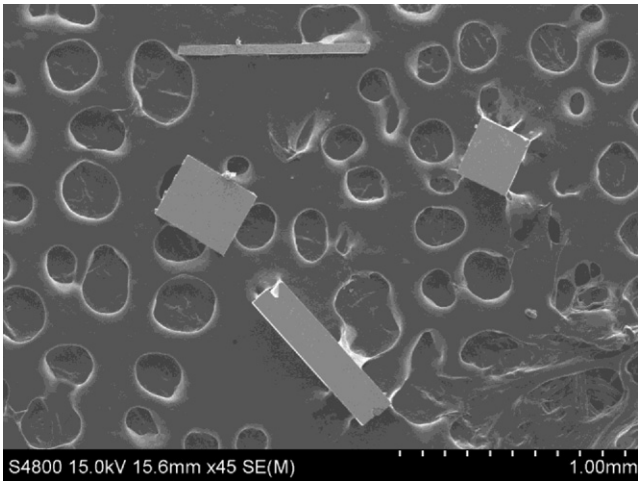

Fig. 2. FESEM micrograph of the obtained single SrB_6 crystals.

conductor, the RRR of the SrB_6 single crystals is very low and the absolute magnitude of ρ is rather large, indicating that the crystals possess semi-metallic conducting behavior. Remarkably, the obvious variation caused by the temperature dependence of resistivity can be observed. The positive slope $\partial\rho/\partial T$ increased with increasing temperature at the temperature range of 2–50 K and 100–300 K; however, it decreased with increasing temperature at the temperature range of 50–150 K. This phenomenon is very similar to that of $CaB_{6-\delta}$ (3N) crystal as reported by Cho et al. [17] (Fig. 3, inset (b)).

To understand the observed metallic conductivity of the SrB_6 single crystal, first principles calculations of the band structure were performed. The conduction band and the valence band are just touching at the X point at the Fermi Level, which supports the experimentally observed conduction behavior of the SrB_6 single crystals (Fig. 4(a)). This result is consistent with that presented in a previous study [9]. The total and partial DOS are presented in Fig. 4(b), which shows that the Fermi level is located in a region of low DOS. From the calculated partial density of states (PDOS) of B and Sr, we can find the states at Fermi level dominantly come from the B 2p states of the octahedral B_6 cluster. In the PDOS of Sr, the Sr 5s and 4d states appear together at the range from 4.5 to 10.7 eV, which indicates the orbital hybridization between Sr 4d and 5s. Comparing the values of Sr 4d and 5s, we know that the hybridized states are mainly made of Sr 4d orbital. Similarly, from the PDOS of B, we can see that the orbital hybridizations between B 2s and 2p appear in the energy ranges of −14.1 to −0.37 eV and

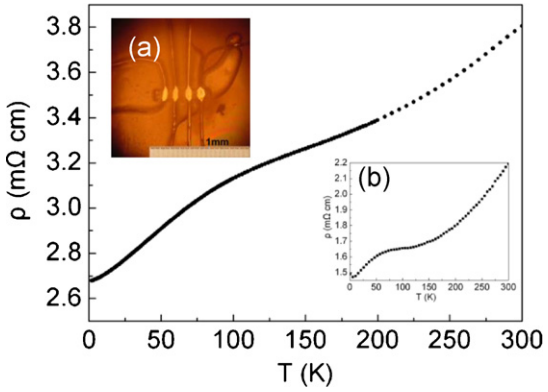

Fig. 3. The resistivity of SrB_6 crystal as a function of temperature; The inset (a) shows a single SrB_6 crystal measured by the conventional four-probe method along the lengthwise direction; The inset (b) presents the resistivity $CaB_{6-\delta}$ (3N) (reported by Cho et al. [17]) crystals as a function of temperature.

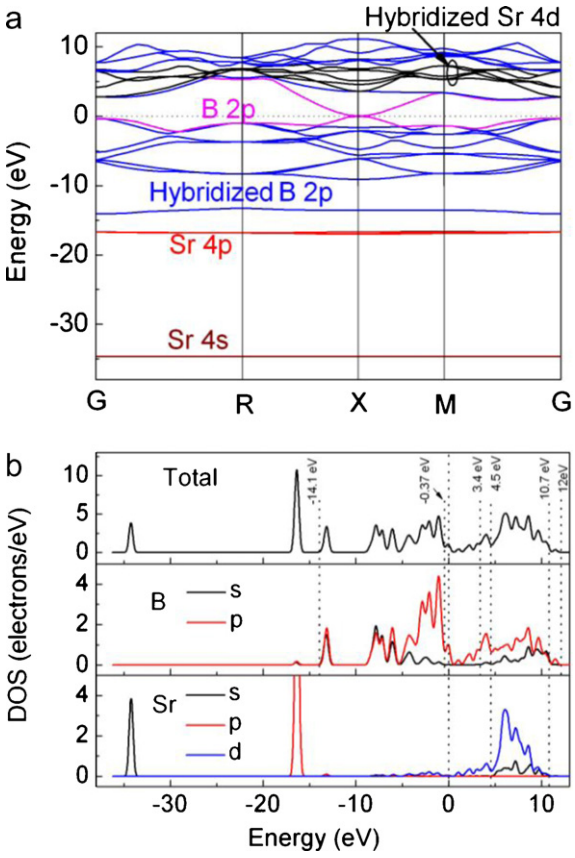

Fig. 4. (a) The calculated band structure of SrB_6 using the CASTEP code. The bands colored with wine, red and black are the 4s, 4p and hybridized 4d orbitals of Sr, respectively; the bands colored with pink and blue are the 2p orbitals and hybridized 2p orbitals of B, respectively. (b) Total and partial DOS of the SrB_6. Dashed line shows the Fermi level. (For interpretation of the references to color in this figure legend, the reader is referred to the web version of this article.)

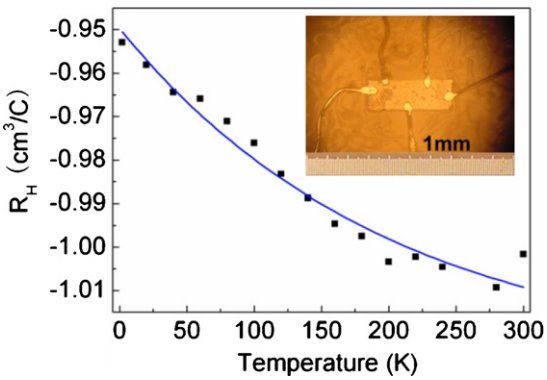

Fig. 5. Hall-coefficient vs. Temperature for SrB_6 single crystal. The inset shows a single SrB_6 crystal measured by the five-point-contact technique along the lengthwise direction.

3.4–12 eV, respectively. This shows that the hybridized B 2p orbitals are split up into two parts: the bonding states below Fermi level in the energy range of −14.1 to −0.37 eV and the antibonding states in the conduction bands from about 3.4 to 12 eV. Basing on the above analysis of PDOS, we confirm the detailed band structures of SrB_6 shown as Fig. 4(a). The conduction bands are made of the 6 hybridized B 2p (blue lines), 5 hybridized Sr 4d (black lines) and 1 B 2p (pink lines) bands. The valence bands are composed of 1 B 2p, 9 hybridized B 2p, 3 Sr 4p and 1 Sr 4s bands. Both the valence band maximum and the conduction band minimum come from B 2p states and intersect at X (1/2, 0, 0) point in the Brillouin zone. On the other hand, the hybridized Sr 4d orbitals are almost located at the conduction bands above the Fermi level in the region higher than 4.5 eV, and have a strong hybridization with the antibonding hybridized B 2p orbitals, which is similar to that of the CaB_6 [9,18–20]. By calculating atomic populations, we analyzed the s–d orbital hybridizations of Sr atoms and found that each Sr atom lost just 1.73 electrons instead of 2 electrons on the 5s orbital for B–B bonding. The s–d orbital hybridizations led to the occupation of 0.58 electrons on the hybridized 4d orbital, which came from the 4s and 5s orbitals (0.58 electrons) of the Sr atom.

Fig. 5 presents the relationship between the Hall coefficient and the temperature of SrB_6 single crystals. The measurement was accomplished using a SrB_6 single crystal measuring 0.38 mm along one axis (Fig. 5, inset). From 2–300 K, the Hall coefficient R_H dropped monotonically with the decreasing temperature. The measured negative Hall coefficients R_H reveal that the conducting carriers are electrons, which mainly come from the 2p orbitals of the B atoms and the 4d orbitals of the Sr atom. The density n of the conducting electrons in SrB_6 single crystals can be estimated using the relation of $R_H = -1/n{\cdot}e$, which is 7×10^{18} electron cm^{-3} at room temperature, i.e., 0.52×10^{-3} free electrons per formula unit.

The room-temperature magnetization measurement indicates the diamagnetic nature of the SrB_6 crystals. The diamagnetic signal in the SrB_6 single crystal is consistent with the fact that Sr ions are divalent with completely filled 4p shells, which is consistent with our calculated results showing that the 4p shell is filled with 5.99 electrons. The susceptibility is -1.60×10^{-9} cm^3 g^{-1}. This

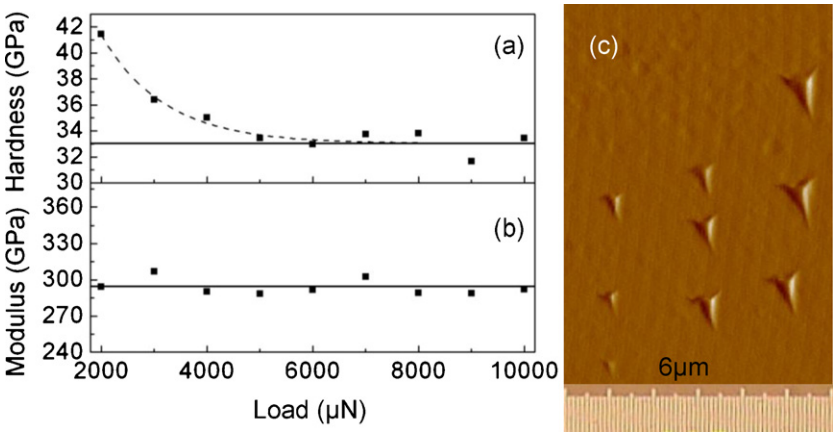

Fig. 6. The hardness (a) and modulus (b) of the SrB_6 as a function of the load on the indenter; (c) AFM image of the indention left by the Berkovich tip on the (1 0 0) face of the SrB_6.

result is in accordance with those that have been reported previously [21,22]. The susceptibility of about -0.22×10^{-6} cm^3 g^{-1} in [21] is much smaller than that found in this study.

The hardness and reduced modulus versus loading for the basic face (1 0 0) of the SrB_6 crystal are shown in Fig. 6(a) and (b), respectively, and the AFM image of the indention is presented in Fig. 6(c). The Exponential Decay curve was fitted from 9 independent measurements. The hardness of the SrB_6 single crystal is 33 GPa, which indicates that SrB_6 is a hard material. The averaged modulus is 293.90 ± 6.55 GPa. Our measured hardness is much higher than that reported by Futamoto et al. (Knoop hardness value: 18.9 ± 0.7 GPa) [23]. This may be attributed to the difference of measuring method and, specifically, the size of the indentation area. In [23], the size of the longer diagonal of indentation is about 40 μm, which is much longer than that in our study (no more than 1 μm for each side of the indentation). Considering the point defects in the crystals, the smaller measuring area has led to more accurate measurement results for hardness. Our result reflects the intrinsic hardness of the SrB_6 single crystals.

4. Conclusions

The SrB_6 single crystals were synthesized under high pressure (5 GPa) and temperature (1300 °C). The SrB_6 possesses cubic structure with $a = 4.1975$ Å, which has been characterized by XRD. The FESEM showed that most of the SrB_6 crystals obtained under these conditions have a rod-like shape with the longest at about 810 μm. Resistivity and the Hall-coefficient measurements showed that the obtained SrB_6 single crystals have a typical semimetal conductive behavior with the electronic conducting carriers. The resistivity and the Hall-coefficient are 3.80 mΩ cm and 7×10^{18} electron cm^{-3} at room temperature, respectively. The calculated band structure shows that the conduction band and the valence band are just touching at the *X* point at the Fermi Level, which confirms the experimentally observed conducting behavior of the SrB_6 single crystal. The total and partial DOS also show that the dominant contributions to the states at the Fermi level come from 2p orbitals of the B atoms and the 4d orbitals of the Sr atom. The magnetization measurement shows that SrB_6 is diamagnetic, which is consistent with the fact that the Sr ion in SrB_6 is divalent with a completely filled 4p shell. In addition, the hardness measurement indicates that SrB_6 is a hard material (33 GPa), and that the averaged reduced modulus value is 293.90 ± 6.55 GPa. Compared with the flux method, the HP–HT method can synthesize pure SrB_6 crystals through only the direct reaction of pure B and Sr elements.

Acknowledgements

This study was funded by the National Natural Science Foundation of China (Grant Nos. 51072174, 50772094 and 50821001) and the NBRPC (Grant No. 2005CB724400).

References

[1] R.M. Adams (Ed.), Boron, Metallo-Boron Compounds, and Boranes, John Wiley & Sons, Inc, New York, 1964.
[2] V.I. Matkovich (Ed.), Boron and Refractory Borides, Springer-Verlag, Berlin, 1977.
[3] D.P. Young, D. Hall, M.E. Torelli, Z. Fisk, J.L. Sarrao, J.D. Thompson, H.R. Ott, S.B. Oseroff, R.G. Goodrich, R. Zysler, Nature (London) 397 (1999) 412–414.
[4] F. Bloch, Z. Phys. 57 (1929) 545–555.
[5] H.R. Ott, J.L. Gavilano, B. Ambrosini, P. Vonlathen, E. Felder, L. Digiorgi, D.P. Young, Z. Fisk, R. Zysler, Physica B 423 (2000) 281–282.
[6] L.S. Dorneles, M. Venkatesan, M. Moliner, J.G. Lunney, J.M.D. Coey, Appl. Phys. Lett. 85 (2010) 6377–6379.
[7] J.D. Denlinger, J.A. Clack, J.W. Allen, G.-H. Gweon, D.M. Poirier, C.G. Olson, J.L. Sarrao, A.D. Bianchi, Z. Fisk, Phys. Rev. Lett. 89 (2002) 157601.
[8] H.R. Ott, M. Chernikov, E. Felder, L. Degiorgi, E.G. Moshopoulou, J.L. Sarrao, Z. Fisk, Z. Phys. B 102 (1997) 337–345.
[9] S. Massidda, A. Continenza, T.M.D. Pascale, R. Monnier, Z. Phys. B 102 (1997) 83–89.
[10] C.O. Rodriguez, R. Weht, W.E. Pickett, Phys. Rev. Lett. 84 (2000) 3903–3906.
[11] D. Hall, D.P. Young, Z. Fisk, T.P. Murphy, E.C. Palm, A. Teklu, R.G. Goodrich, Phys. Rev. B 64 (2001) 233105.
[12] S. Muranaka, S. Kawai, J. Crystal. Growth 26 (1974) 165–168.
[13] G. Balakrishnan, M.R. Lees, D.M.K. Paul, J. Crystal. Growth 256 (2003) 206–209.
[14] P. Jash, A.W. Nicholls, R.S. Ruoff, M. Trenary, Nano Lett. 8 (2008) 3794–3798.
[15] Z.Y. Liu, X.Y. Han, D.L. Yu, Y.X. Sun, B. Xu, X.F. Zhou, J.L. He, H.T. Wang, Y.J. Tian, Appl. Phys. Lett. 96 (2010) 031903.
[16] W.C. Oliver, G.M. Pharr, J. Mater. Res. 19 (1) (2004) 3.
[17] J.S. Rhyee, B.K. Cho, J. Appl. Phys. 95 (2004) 6675–6677.
[18] K. Schmitt, C. Stuckl, H. Ripplinger, B. Albert, Solid State Sci. 3 (2001) 321–327.
[19] B. Lee, L.W. Wang, Appl. Phys. Lett. 87 (2005) 262509.
[20] L.H. Li, L. Chen, J.Q. Li, L.M. Wu, J. Phys. Chem. C 113 (2009) 15384–15389.
[21] J. Etourneau, J.P. Mercurio, R. Naslain, P. Hagenmuller, J. Solid State Chem. 2 (1970) 332–342.
[22] K. Taniguchi, T. Katsufuji, F. Sakai, H. Ueda, K. Kitazawa, H. Takagi, Phys. Rev. B 66 (2002) 064407.
[23] M. Futamoto, T. Aita, U. Kawabe, Mater. Res. Bull. 14 (1979) 1329.